Variation of the physicochemical and morphological characteristics of solvent casted poly(vinylidene fluoride) along its binary phase diagram with dimethylformamide

J.C.C. Ferreira [a], T.S. Monteiro [a], A.C. Lopes [a], C.M. Costa [a], M.M. Silva [b], A.V. Machado [c], S. Lanceros-Mendez [a,*]

a Centro/Departamento de Física, Universidade do Minho, 4710-057 Braga, Portugal

[b] Centro/Departamento de Química, Universidade do Minho, 4710-057 Braga, Portugal

[c] IPC - Institute for Polymers and Composites/I3N, Universidade do Minho, Campus de Azurém, 4800-058 Guimarães, Portugal

Keywords:

PVDF;
Porous membranes;
Solvent casting;
Phase diagram;
Mesoscale simulation

Abstract

Poly(vinylidene fluoride), PVDF, films and membranes were prepared by solvent casting from dimethylformamide, DMF, by systematically varying polymer/solvent ratio and solvent evaporation temperature. The effect of the processing conditions on the morphology, degree of porosity, mechanical and thermal properties and crystalline phase of the polymer was evaluated. The

obtained microstructure is explained by the Flory-Huggins theory. For the binary system, the porous membrane formation is attributed to a spinodal decomposition of the liquid-liquid phase separation. The morphological features were simulated through the correlation between the Gibbs total free energy and the Flory-Huggins theory. This correlation allowed the calculation of the PVDF/DMF phase diagram and the evolution of the microstructure in different regions of the phase diagram. Varying preparation conditions allow tailoring polymer microstructure while maintaining a high degree of crystallinity and a large β crystalline phase content. Further, the membranes show adequate mechanical properties for applications in filtration or battery separator membranes.

Introduction

Membrane technology is widely used in biomedical [1], chemical [2], filtration [3] and energy storage [4] applications, among others. Each application imposes specific membrane characteristics such as porosity, pore size distribution, roughness and permeability, among others [5,6].

Fluoropolymers are particularly interesting for the preparation of porous membranes for different applications and, in particular, poly(vinylidene fluoride), PVDF, and its copolymers are appealing due to their suitable mechanical properties, high dielectric response, high thermal stability, chemical inertness and hydrophobic properties [7-10].

The hydrophobic characteristic of PVDF is essential for membrane distillation applications, for example. PVDF is soluble in most aprotic solvents such as N,N-dimethylacetamide (DMAc), N,N-dimethylformamide (DMF), N-methyl-2-pyrrolidone (NMP), dimethylsulfoxide (DMSO) and triethylphosphate (TEP) [5,11].

PVDF membranes can be prepared by phase inversion processes such as thermal evaporation, immersion precipitation, non-solvent separation and electrospinning [12-16]. The membrane formation is influenced by the polymer concentration, solvent temperature evaporation, solvent type, non-solvent content in the solution and coagulation bath [17,18].

A wide variety of porous morphologies can be obtained through the combination of these processing parameters [5]. The selection of the solvent is critical in order to tailor the porous structure, as it controls the pore growth kinetics and the crystallization behavior of the polymer.

The morphologies of the membranes can be predicted by analyzing the phase diagram of the system. The phase diagram for a two or three component system (polymer, solvent and non-solvent) shows the regions of miscibility and the regions where the phase separation occurs [19]. The formation of pores - cellular or finger-like - in the membrane can be obtained in the liquid-liquid event (binodal line in the phase diagram) whereas interlinked crystalline phase prevails in solid-liquid phase [11]. In particular, the mechanical properties of the membranes are strongly dependent on porosity and pore size and polymer membranes with high degree of porosity and large pores often does not show adequate properties to be used in demanding membrane applications.

Large values of porosity are obtained with a high level of miscibility between solvent and non-solvent, which will influence the demixing rate and therefore the final microstructure

[6]. Another critical parameter is the polymer concentration as it affects the solution thermodynamic properties such as the binodal line. Most often the polymer concentration when a sample is prepared by solvent casting is between 15 and 25wt.%. Increasing polymer concentration in the solution results in membranes with lower porosity and higher interface between polymer and nonsolvent [20]. Finally, temperature also strongly affects membrane formation. The viscosity of the solution and the exchange rate of solvent and non-solvent during phase inversion can be controlled through temperature [21,22]. Through temperature variations it is also possible to determine the cloud-point that represents an approximate boundary when liquid-liquid demixing occurs.

Microporous membranes of PVDF have been prepared by precipitation from 1-octanol/DMF/PVDF and water/DMF/PVDF systems. It was verified that as the temperature increases, the gelation region contracts significantly more than the liquid-liquid demixing region. Cellular asymmetric morphologies were obtained at high temperatures [21].

PVDF membranes were also produced from DMA/water and DMA/ C1-C8 alcohols solvent/non-solvent pairs, concluding that high casting solution temperatures play an important role in membrane formation due to the effect of increasing liquid-liquid demixing rate on the crystallization [17].

Polymer membranes were also achieved from PVDF/DMSO/water [23] and PVDF/DMAc/water systems [18]. Membranes show low degree of crystallinity and the presence of both α - and β-phases in the surface layers when precipitated at high temperatures.

The microstructure of PVDF can be also modified by crystallizing from binary systems, such as PVDF/DMF at different temperatures, the solvent evaporation playing a critical role for obtaining porous membranes based on PVDF [14].

In this sense, PVDF membranes with TEP as a solvent have been prepared for micro- and ultra-filtration, showing that symmetric and asymmetric structures with bi-continuous inter-connected pores can be effectively controlled by tuning PVDF concentration [11].

Computer simulation of the polymer structure ("mesoscale structure") is very important for predicting and understanding the microstructure formation at different points of the phase diagram in binary or ternary systems [24]. The morphology is obtained through mesoscale modeling of the polymer/solvent interaction [25].

Despite the aforementioned efforts in modifying PVDF microstructure, a systematic approach along binary phase diagrams is still needed, being nevertheless the simplest way to obtain specific microstructure in a systematic and reproducible way. In the present work, PVDF membranes were prepared by solvent casting from a binary system with N , N dimethylformamide (DMF) as a solvent varying polymer/solvent relative content and evaporation temperature.

The effects of polymer concentration and solvent evaporation temperature were thus systematically studied and the phase diagram of the polymer solution was analyzed according to the Flory-Huggins theory. The microstructure of the PVDF/DMF binary system in different points of the phase diagram was simulated through mesoscopic

models. Membranes with different microstructures, degree of crystallinity, crystalline phase content, porosity and mechanical properties have been obtained.

Experimental

Materials

PVDF (Solef 1010 with Mw = 352,000 g/mol) was supplied by Solvay. The solvent N,N-dimethylformamide (DMF, 99.5%) was purchased from Merck.

Membrane preparation

The PVDF concentration in solution ranged between 5wt.% and 20wt.%. The polymer was dissolved in DMF at room temperature using a magnetic stirrer until a homogeneous solution was obtained. After total dissolution of the polymer, flexible films of $\sim 50\mu$ m were obtained by spreading the solution on a clean glass substrate followed by isothermal evaporation in a temperature range between room temperature and 80°C within an air oven of Binder during the maximum 15 days. The samples produced were called (x PVDF y) where x represents the polymer concentration and y represents the evaporation solvent temperature.

Sample characterization

The porosity of the samples ($\emptyset$) was measured with a pycnometer by the following procedure: the weight of the pycnometer filled with ethanol was measured and labeled as (W_1); the mass of the sample was measured (Ws) and immersed in ethanol. After the sample was soaked in ethanol, additional ethanol was added to complete the volume of the pycnometer. Then, the pycnometer was weighted and labeled as (W_2) and the sample filled with ethanol was taken out of the pycnometer. The residual weight of the ethanol and the pycnometer was labeled (W_3). The porosity of the membrane was calculated according to [26]:
$\phi = \frac{W_2 - W_3 - W_S}{W_1 - W_3}$.
The mean porosity of each membrane was obtained as the average of the values determined in three samples and the error is given as the standard deviation of the values.

The morphology of the PVDF membranes was analyzed by scanning electron microscopy (SEM) (Cambridge, Leica) with an accelerating voltage of 15 kV . Previously the samples were coated with a thin gold layer using a sputter coating (Polaron, model SC502 sputter coater).

The polymer phase within the porous membranes was determined by Fourier Transformed Infrared Spectroscopy (FTIR) performed at room temperature with a Perkin-Elmer Spectrum 100 apparatus in ATR mode from 4000 to 650 cm^{-1}. FTIR spectra were collected after 32 scans with a resolution of 4 cm^{-1}.

The thermal behavior and degree of crystallinity of the PVDF membranes were analyzed by differential scanning calorimetry (DSC) measurements with a Mettler DSC 821 (Mettler-Toledo) apparatus. The samples were cut into small pieces, placed into 50μl

aluminum pans and heated between room temperature and 200°C at a heating rate of 10°C/min. All experiments were performed under a nitrogen purge. The temperature accuracy of the thermal analyzer is ±0.1°C.

Mechanical tests were carried out at room temperature through stress-strain measurements in the tensile mode of a TST350 setup from Linkam Scientific Instruments and a strain rate of 15μ m/s. The tensile force range of the instrument ranges from 0.01 N to 20 N with a force resolution of 0.001 N .

The estimated error in the FTIR, DSC and mechanical tests was calculated taking into account the precision of the equipment and the least squares method.

Mesoscale simulation method

The phase separation phenomena in the polymer mixture were described by phenomenological mesoscopic models based on dynamic density functional.

The concept behind the mesoscale model is the Gibbs free energy, F, described as a functional:

$$F = F^{id} + F^{mf} \tag{2}$$

where F^{id} is the ideal free energy function and F^{md} is the mean field free energy.

The dynamic density functional model consists on representing the total functional free energy in order of time. This model is represented by the diffusion equation of the time-dependent Ginzburg-Landau model [27]:

$$\frac{\partial c(r,t)}{\partial t} = \frac{M\nabla^2 \delta F}{\delta c(r,t)} + \eta(r,t) \tag{3}$$

where c is the volume fraction of the polymer, M is the kinetic coefficient and $\eta(r,t)$ is a Gaussian random force.

The simulation was performed through the MesoDyn Model of Materials Studio software v6.0.0. The size of the box was 200 × 200 × 32 nm with a number of simulation steps of 2000. For the morphology simulation, polymer mixture was defined through creation of the amorphous cell before submitting the cell to temperature variation. Finally, the variation of the degree of porosity (phase-separation) was studied as a function of the volume fraction of the polymer within the solution and the solvent evaporation temperature independently of the size of the box. [24].

Results

Fig. 1 shows SEM images of the cross section morphologies for the membranes prepared by solvent casting with 20wt. % of PVDF in DMF at room temperature (Fig. 1a), 40°C (Fig. 1b) and 80°C (Fig. 1c).The membranes show different morphologies, ranging from a porous (Fig. 1a) to a dense microstructure (Fig. 1b and c). Fig. 1a shows a three dimensional fibriform network suggesting a precipitation situation dominated by liquid-liquid demixing in the phase diagram [28]. For the higher crystallization

temperature above 40°C, the membranes (Fig. 1b and c) exhibit a more dense morphology due to the larger spherulite diameter (surface microstructure not reported). At higher temperatures, the polymer chains have enough mobility to occupy the free space left by the solvent during evaporation, leading to a more compact structure. These phenomena can be observed in Fig. 1c and d for the same evaporation temperature ($T = 80°C$) and different polymer concentrations, 20wt. % and 5wt. %, respectively. The porosity observed in Fig. 1d is the result of the free space between spherulites with high diameter. These microstructural variations are fully ascribed to the different solvent evaporation rates and polymer chain mobility during crystallization and can be observed along the cross-section of all samples (Fig. 1a, b and c), indicating a homogeneous solvent evaporation.

The effect of PVDF concentration for a given evaporation temperature (40°C and 80°C) on membrane morphology is also presented in Fig. 1. While Fig. 1c and *d* represents samples prepared with 5wt. %

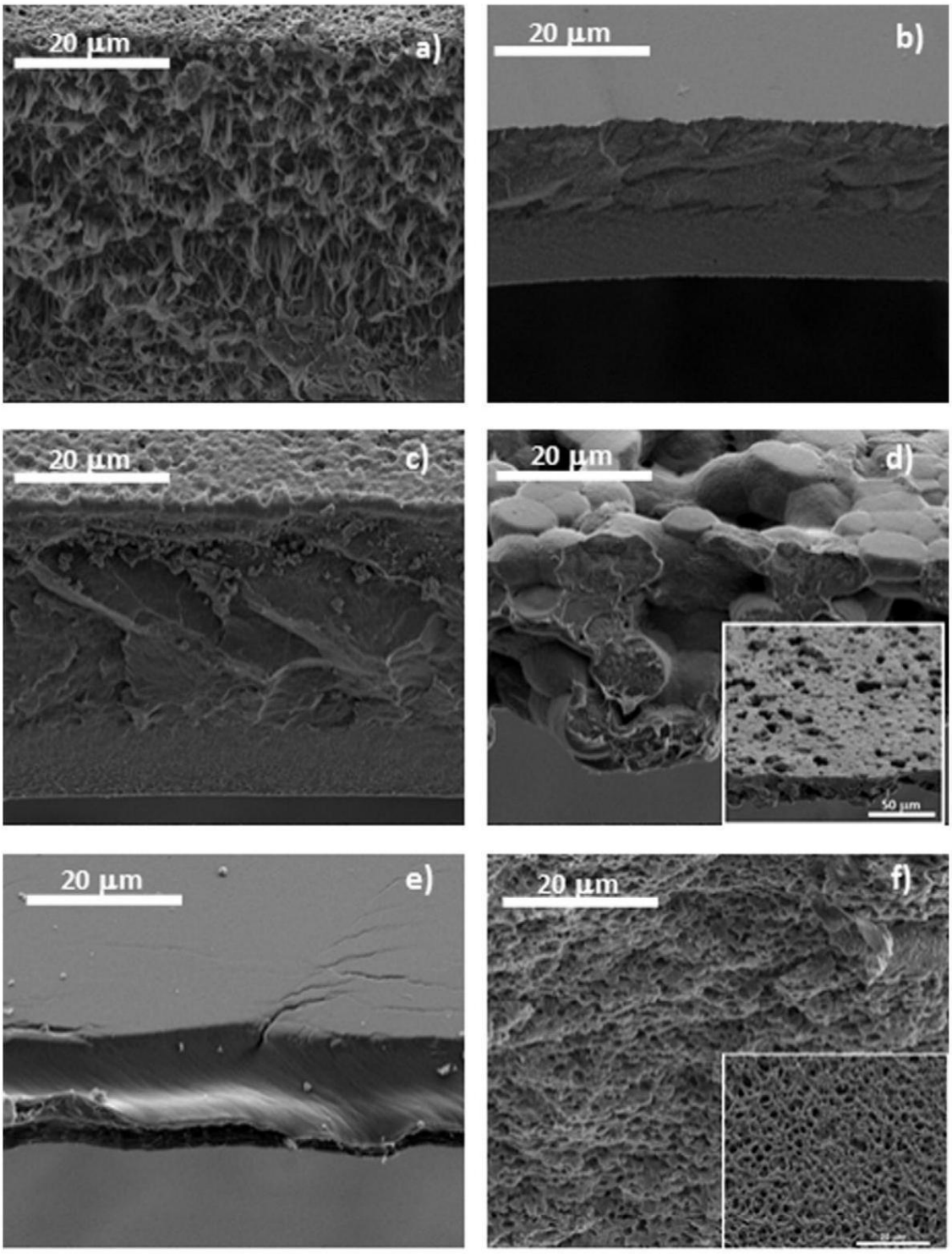

Fig. 1. Cross-section images of the PVDF membranes prepared from a PVDF/DMF solution with 20wt% of PVDF at: room temperature (a), 40°C (b) and 80°C (c). With 5wt. % of PVDF at 80°C (d) and at 40°C in the PVDF/DMF solution with 5wt. % of PVDF (e) and 15wt. % of PVDF (f). Inset of panels d and f represents the surface of the samples.

Table 1
Degree of porosity of the membranes as a function of the preparation conditions. In the sample identification, the first number corresponds to the polymer weight content and the second to the solvent evaporation temperature.

Sample	Porosity /±5%
20 PVDF 25	70
20 PVDF 80	9
5 PVDF 80	17
5 PVDF 40	0
15 PVDF 40	79

and 20wt. % contents of PVDF in PVDF/DMF and solvent evaporation at 80 °C, Fig. 1e and f shows the cross-section images for 5wt. % and 15wt. % contents of PVDF in PVDF/DMF at an evaporation temperature of 40°C. Independently of the solvent evaporation temperature, the influence of polymer concentration in sample morphology is relatively large (Fig. 1). At low polymer concentration (5 wt.%) and at 40 °C (Fig. 1e) a compact microstructure is observed that evolves to a particulate morphology with macrovoids or finger-like pores for samples prepared from 15wt. % polymer concentration (Fig. 1f). Concerning the effect of PVDF concentration on solvent evaporation at higher temperatures (80°C), a particular morphology is observed with globular particles distributed uniformly in the membrane prepared with 5wt. % of PVDF. It has a denser microstructure than the membrane prepared with 20wt. % PVDF. This behavior is attributed to the initial position of the solution in the phase diagram of the PVDF/DMF system (see later). As shown in Fig. 1, the evaporation temperature of the solvent strongly affects the effect of PVDF concentration on membrane morphology. The porosity of the above presented membranes is summarized in Table 1.

As evidenced in Table 1 and supported by Fig. 1, for high content of the PVDF concentration in the PVDF/DMF system, the porosity decreases as the evaporation temperature increases. For the lower crystallization temperatures, the polymer chains show a reduced mobility, hindering the polymer to occupy the free space left by the evaporated solvent. The obtained microstructure is therefore characterized by an elevated porosity and polymer crystallized with a small spherulitic radius. Polymer diffusion and spherulite growth are favored with increasing temperatures [14] leading to a more compact microstructure.

For a given solvent evaporation temperature, the polymer concentration has relevant role in morphology and degree of porosity of the PVDF membranes, leading to a larger degree of porosity as the polymer concentrations increases. These effects will be later discussed taking into account the phase diagram of the binary system.

Together with the membrane morphology, it is relevant to consider the resulting crystalline phase of the polymer after polymer crystallization; as it can show polar and non-polar phases, which is relevant for different applications. The FTIR-ATR spectra of the PVDF membranes prepared by solvent evaporation at different temperatures and different relative polymer contents at a

given temperature are shown in Fig. 2a, together with the identification of the specific band characteristics of the α-phase (765,796 and 976 cm^{-1}) [10] and β-phase (840 cm^{-1}) [10] of the polymer. No other polymer phase can crystallize under the present preparation conditions [29].

The α and β phase contents were quantified using the bands at 766 cm^{-1} and 840 cm^{-1}, that have been identified as representative of the α - and β-phases, respectively, and the method presented in [10, 30,31]. Shortly, the phase content was calculated from the FTIR spectra by applying [10,32].

$$F(\beta) = \frac{X_\beta}{X_\alpha + X_\beta} = \frac{A_\beta}{(K_\beta/K_\alpha)A_\alpha + A_\beta} \quad (4)$$

where, $F(\beta)$ represents the β-phase content; A_α and A_β are the absorbencies at 766 and 840 cm^{-1}, corresponding to the α and β phases, respectively ; $K_\alpha(6.1 \times 10^4\ cm^2/mol)$ and $K_\beta(7.7 \times 10^4\ cm^2/mol)$ are the absorption coefficients at the respective wave number and X_α and X_β are the degree of crystallinity of each phase.

The degree of crystallinity of each sample was calculated through the weight fraction of the α - and β-phases considered in the FTIR measurements and the melting enthalpy of the samples obtained from DSC (Fig. 2b) and the melting enthalpy of pure crystalline α - and β-phase PVDF which is reported to be 93.04 J/g and 103.4 J/g respectively [33] through the following equation:

$$\chi_C = \frac{\Delta H_f}{x\Delta H_\alpha + y\Delta H_\beta} \quad (5)$$

where x and y are the weight fractions of the α and β phases as determined from the FTIR measurements (Fig. 2a), ΔH_α is the melting enthalpy of pure crystalline α-PVDF and ΔH_β is the melting enthalpy of pure crystalline β-PVDF.

The β-phase fraction, melting temperature and degree of crystallinity of the obtained membranes are summarized in Table 2.

Table 2 shows that a high β-phase crystalline fraction is obtained in the samples independently of the preparation conditions of the PVDF membranes in the PVDF/DMF system.

Thus, independently of the initial polymer concentration and for solvent evaporation temperatures up to 80°C, the nucleation of the β phase is promoted [10]. Significant chain entanglements lead to an oriented packing of $CH_2 - CF_2$ dipoles favoring the formation of the β-phase crystals [23]. The evaporation rate is essential in determining the obtained crystalline phase [10,30,34,35].

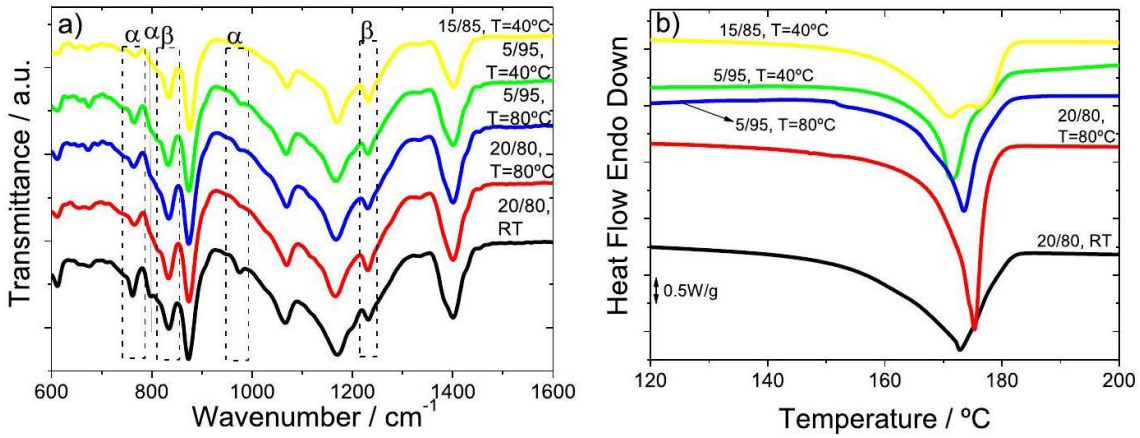

Fig. 2. a) FTIR-ATR spectra and b) DSC thermograms for the PVDF membranes prepared under the different conditions. In the sample identification, the first number corresponds to the polymer weight content and the second to the solvent evaporation temperature.

The DSC thermograms of the different samples are shown in Fig. 2b. The melting behavior of the membranes is similar and characterized by a broad melting peak at 171 °C – 175°C, as presented in Table 2. The samples crystallized from a 20wt. % PVDF content at different temperatures, and the larger melting peak width of the PVDF membrane crystallized at room temperature indicates a more defective crystalline structure and a larger distribution of crystallite sizes when compared to the samples prepared after evaporation at higher temperatures [36,37]. The degree of crystallinity is also nearly independent of the processing temperature, just the sample prepared from 5wt. % of PVDF and evaporated at 40°C showing a lower degree of crystallinity (Table 2). Fig. 2b and Table 2 demonstrate that, within experimental error, the melting temperature of PVDF membranes is not affected by the evaporation temperature of the solvent and the polymer concentration.

For certain applications, such as, filtration and battery separators the mechanical properties that are related to integrity and safety of the materials are a critical factor, being these strongly affected by the porous microstructure [38]. In the stress-strain curves (Fig. 3) the most relevant parameters are the elastic modulus (slope of stress-strain in the elastic region at a deformation of 5%) and the yielding stress (limiting the elastic and plastic regions) [39].

The stress-strain curves for the PVDF membranes are represented in Fig. 3 and the resulting mechanical parameters are summarized in Table 3. Independently of the processing conditions and the resulting microstructure, the stress-strain curves (Fig. 3) show the two well defined regions indicative of an elastic and plastic deformation regimes.

The morphological differences (Fig. 1) are nevertheless reflected in the mechanical properties of the PVDF membranes, the elastic modulus of the PVDF membranes increasing from 0.3 GPa to 1.5 GPa with increasing evaporation temperature. Furthermore, the yielding stress of 20wt. % of PVDF at a solvent evaporation temperature of 80°C is 51 MPa , this is similar to the values obtained for PVDF films due to the low degree of porosity [40].

The increase of polymer concentration in the initial PVDF/DMF solution affects membrane porosity and degree of crystallinity (Tables 1 and 2), which is reflected in the mechanical properties (Table 3). For a given degree of crystallinity (55%) for samples

prepared from 20wt.% PVDF solutions at different solvent evaporation temperatures (room temperature and 80°C), it is observed that the Young modulus and yielding stress increase with decreasing degree of porosity. Thus, the Young modulus and yielding stress for samples prepared from 5wt.% of PVDF in the initial solution are 2.6 GPa and 40 MPa, which are higher than 1.4 GPa and 19 MPa of the samples prepared from 15wt.% PVDF content, which is related to the differences in porosity and microstructure.

Discussion

The microstructure of the polymer obtained by processing the samples at different PVDF initial solution concentrations and solvent evaporation temperatures is shown in Fig. 1. The different microstructures are due to the phase separation, solvent evaporation and polymer crystallization during membrane preparation as it is illustrated in the phase diagram of Fig. 4b. Independently of the PVDF initial concentration and solvent evaporation temperature, the membranes show high

Table 2

β-Phase fraction, melting temperature (T_m) and degree of crystallinity (χ) of the membranes as a function of the preparation conditions. In the sample identification, the first number corresponds to the polymer weight content and the second to the solvent evaporation temperature.

Sample	β-Phase /$\pm$2%	T_m/$\pm$1 °C	χ/$\pm$5%
20 PVDF 25	65	173	55
20 PVDF 80	77	175	55
5 PVDF 80	75	174	59
5 PVDF 40	70	172	40
15 PVDF 40	80	171	60

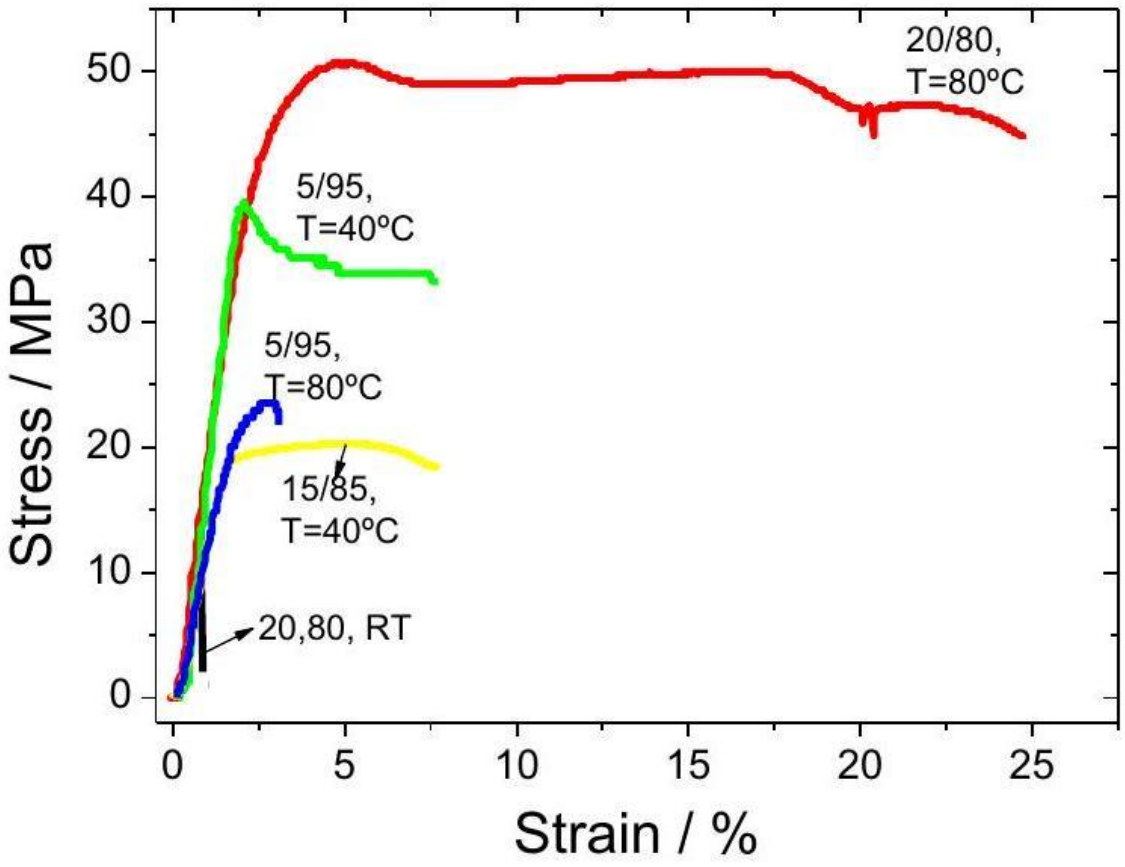

Fig. 3. Stress-strain behavior for the different PVDF membranes. In the sample identification, the first number corresponds to the polymer weight content and the second to the solvent evaporation temperature.
content of the β-phase fraction above 65% (Fig. 1a), which is fully related to the low solvent evaporation temperature [10]. Small differences observed in the degree of crystallinity, as determined by the DSC (Fig. 2b) and the mechanical properties mainly depend on the evaporation temperature as they are mainly affected by the porosity.

The isothermal evaporation process can be described by the FloryHuggins theory [41]. The phase diagram is obtained from the derivation of the free energy and the phase behavior of the polymer-solution at the upper critical solution temperature (UCST). The UCST is the critical temperature above which the components of a mixture are miscible in all proportions.

The phase diagram (Fig. 4b) shows the regions of stability, metastability and instability of the polymer solution. The energy fluctuations are described by [42]:

$$\frac{\Delta G_m}{RT}\sum \frac{\phi_i}{N_i}\ln\,\phi_i + \sum \chi_{ij}\phi_i\phi_j \qquad (6)$$

where ϕ_{ij} is the volume fraction of the components, χ_{ij} is the Flory-Huggins interaction parameters and N_i is the degree of polymerization.

For a polymer/solvent binary system Eq. (6) is rewritten as [43]: $\frac{\Delta G}{RT} = \frac{\phi_1}{n}\ln\ \phi 1 + \phi_2 \ln\ \phi_2 + \chi_{12}\phi_1\phi_2$.

Assuming that

$$\phi' = \phi_1, \phi_2 = 1 - \phi' \tag{8}$$

the free energy variation of the binary mixture as a function of the polymer volume fraction can be expressed as

$$\frac{\Delta G}{RT} = \frac{\phi'}{n}\ln\ \phi' + (1-\phi')\ln\,(1-\phi') + \chi_{12}\phi'(1-\phi') \tag{9}$$

Table 3
Mechanical properties of the different PVDF membranes. In the sample identification, the first number corresponds to the polymer weight content and the second to the solvent evaporation temperature.

Sample	Young modulus/GPa ±2%	Yielding stress/MPa ±2%
20 PVDF 25	0.3	14
20 PVDF 80	1.5	51
5 PVDF 80	1.4	24
5 PVDF 40	2.6	40
15 PVDF40	1.4	19

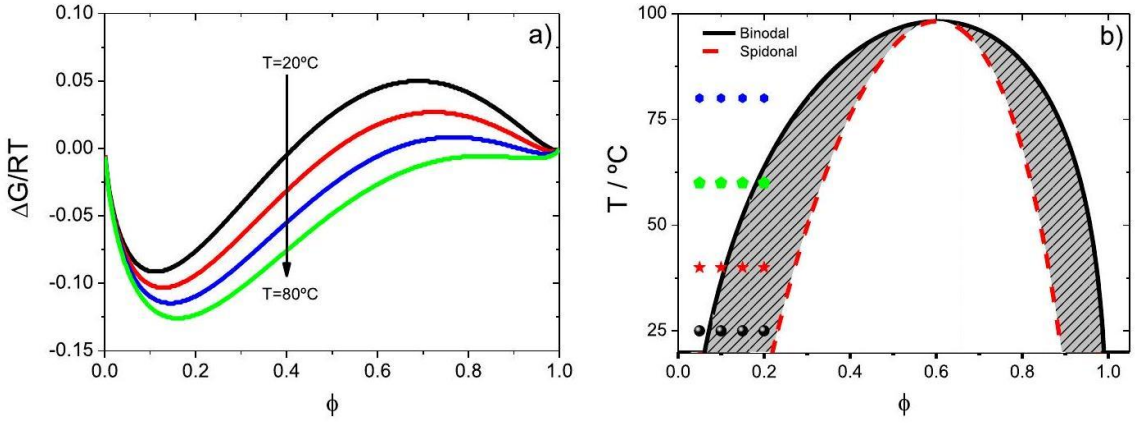

Fig. 4. a) Variation of the Gibbs free energy and b) variation of the spinodal and binodal temperatures as a function of volume fraction $\varphi = \varphi_{\mathrm{PVDF}}$ for the PVDF/DMF system. where n is the degree of polymerization, ϕ' is the polymer volume fraction and χ_{12} is the Flory-Huggins parameter for a binary mixture.

By derivation of the free energy in order to ϕ', the chemical potential μ' is obtained: $\frac{\partial \frac{G}{RT}}{\partial \phi'} = \mu' = \frac{\ln\ \phi' + 1}{n} - \left(1 + \ln\,(1-\phi') + \chi_{12}\phi'(1-\phi')\right)$.

Defining the phase boundary by the calculation of the common tangent of the free energy corresponding to ($\mu_1 = \mu_2$) and solving numerically this equation in order to χ_{12}, the binodal line is obtained [44].

The Flory-Huggins parameter χ_{12} in order to temperature is expressed as:

$$\chi_{12} = \frac{v_0}{RT}\delta^2 \tag{11}$$

where R is the gas constant, v_0 is the molar volume of the solvent, T is the temperature, and δ is the solubility parameter.

Based on the Flory Huggins theory (Eqs. (6)-(11)) and its application to the PVDF/DMF system, the Gibbs free energy density (ΔG) and the phase diagram have been constructed, as shown in Fig. 4a, using $v_0 = 77.4\ \mathrm{cm}^3 \cdot\ \mathrm{mol}^{-1}$ (DMF volume molar), $N = 5.5$ (Solvay datasheet) and the solubility parameters ($\delta = \delta_{\mathrm{PVDF}} - \delta_{\mathrm{DMF}} = 7.4$) [45].

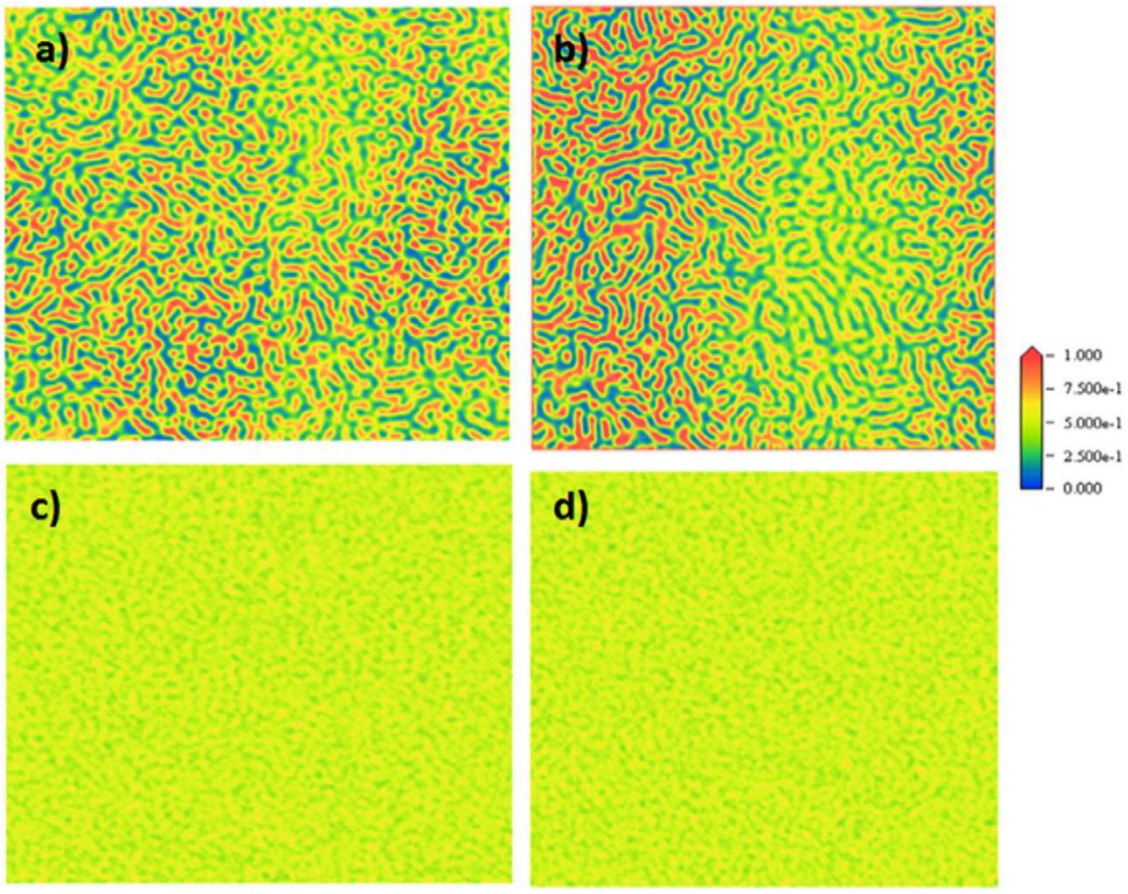

Fig. 5. Representation of the PVDF microstructure in the PVDF/DMF system at 25°C for a) 5% of PVDF and b) 20% of PVDF and at 80 °C for c) 5% of PVDF and d) 20% of PVDF in the initial solution. The color-code represents the variation of the density on the system (polymer/solvent) in which red represents a higher density and blue a lower density.

Fig. 4a shows the variation of free energy of mixing (ΔG) as a function of polymer content in the PVDF/DMF system. It can be noticed that for miscibility to occur, ΔG must be smaller than 0 and that its behavior is strongly dependent on temperature [44], the miscibility of the system increasing with increasing temperature.

The phase separation can be thus controlled through the polymer/ solvent ratio, the solvent evaporation temperature and the thermal diving force as shown in the phase diagram of Fig. 4b, characterized by the binodal and spinodal lines.

The binodal line (black line in Fig. 4b) corresponds to generalized phase separation and the spinodal line (red line in Fig. 4b) relates to the onset of density fluctuations leading to phase separation. The metastable region between the spinodal and binodal lines is referred to the nucleation and growth region [46]. The phase separation occurs either by spinodal decomposition or by nucleation and growth (metastable region). The initial sample preparation conditions (polymer concentration and solvent evaporation temperature) are represented by the symbols in the phase diagram of Fig. 5.

For a polymer/solvent ratio at solvent temperatures of $20°C$ and $80°C$ the system is in the metastable region where it undergoes growth and nucleation of the diluted polymer phase. The solvent evaporation at $80°C$ is at the limit for the presence of the porosity in the PVDF/DMF system. For temperatures at or above $80°C$ the one-phase region is verified (homogeneous microstructure) and a non-porous microstructure is observed (Fig. 1).

At solvent evaporation at $40°C$ for the different polymer/solvent ratios, the microstructure formation is governed by a competition between the phase separation dynamics and the solvent evaporation rate. When the polymer concentration is increased in the PVDF/DMF solution, the system transits from the unstable (5wt. % of PVDF) to the metastable region (15wt. % of PVDF) in which the process is dominated by spinodal decomposition. For this reason, the microstructure of the PVDF membrane changes from a homogeneous to a heterogeneous microstructure (Fig. 1).

The phase separation process and the morphology formation were simulated in different regions of the PVDF/DMF phase diagram, as shown in Fig. 5. The surface image is divided between two phases and the color-code represents the variation of the density on the system (polymer/solvent) in which red represents a higher density and blue a lower density.

Fig. 5a and b shows the morphology obtained at room temperature in the zone between the binodal and spinodal lines, where phase separation occurs.

By comparison of Figs. 5 and 1, a correlation is observed between the experimental results and obtained microstructure in the simulations. Fig. 5 shows the phase separation when the solvent is evaporated at room temperature and that the phase separation depends on the dilution of the solution. The microphase separation (Fig. 5a) is lower in the more diluted solution and increases with increasing PVDF content (Fig. 5a and b). At high evaporation temperature ($T = 80°C$), but different polymer concentration (Fig. 5c, 5wt. % of PVDF and Fig. 5d, 20wt. % of PVDF), these points are located outside of the binodal line and no liq-uid-liquid phase separation is observed.

Finally, the factor that affects more the phase separation, as observed in Fig. 5, is the solvent evaporation temperature when compared to polymer concentration.

Conclusions

Poly(vinylidene fluoride), PVDF, membranes were prepared by solvent casting varying processing parameters such as polymer/solvent ratio and solvent evaporation temperature. PVDF membranes with different morphologies were produced by changing those parameters. The phase diagrams for the binary system are obtained by the FloryHuggins theory and the obtained microstructure is correlated with the experimental results. The porous microstructure is attributed to spinodal decomposition of the liquid-liquid phase separation. The results show that the PVDF membranes show degrees of crystallinity around 50% and a large β-phase content.

Acknowledgment

This work was supported by FEDER through the COMPETE Program and by the Portuguese Foundation for Science and Technology (FCT) in the framework of the Strategic Project PEST-C/FIS/UI607/2013, PEST-C/ QUI/UI0686/2013 and the project PTDC/CTM-NAN/112574/2009. A.C.L. and C.M.C. thank the support of the FCT (grant SFRH/BD/62507/2009 and SFRH/BD/68499/2010). The authors also thank the support from the COST Action MP1003, 2010 'European Scientific Network for Artificial Muscles' and funding from Matepro-Optimizing Materials and Processes, ref. NORTE-07-0124-FEDER-000037, co-funded by the "Programa Operacional Regional do Norte" (ON.2-O Novo Norte), under the "Quadro de Referência Estratégico Nacional"(QREN), through the "Fundo Europeu de Desenvolvimento Regional" (FEDER). The authors also thank the Departamento de Física Química, Universidad del País Vasco, Spain, for hosting part of this research.

References

[1] S.P. Adiga, C. Jin, L.A. Curtiss, N.A. Monteiro-Riviere, R.J. Narayan, Nanoporous membranes for medical and biological applications, Wiley Interdiscip. Rev. Nanomedic. Nanobiotechnol. 1 (2009) 568-581.
[2] R. Baker, Membrane Technology and Applications, Wiley, 2012.
[3] P. Eriksson, Nanofiltration extends the range of membrane filtration, Environ. Prog. 7 (1988) 58-62.
[4] C.M. Costa, L.C. Rodrigues, V. Sencadas, M.M. Silva, J.G. Rocha, S. Lanceros-Méndez, Effect of degree of porosity on the properties of poly(vinylidene fluoridetrifluorethylene) for Li-ion battery separators, J. Membr. Sci. 407-408 (2012) 193-201.
[5] G.R. Guillen, Y. Pan, M. Li, E.M.V. Hoek, Preparation and characterization of membranes formed by nonsolvent induced phase separation: a review, Ind. Eng. Chem. Res. 50 (2011) 3798-3817.
[6] M. Mulder, Basic Principles of Membrane Technology, Kluwer Academic, 1996.
[7] M. Khayet, C.Y. Feng, K.C. Khulbe, T. Matsuura, Preparation and characterization of polyvinylidene fluoride hollow fiber membranes for ultrafiltration, Polymer 43 (2002) 3879-3890.
[8] J.M. Ortiz de Zárate, L. Peña, J.I. Mengual, Characterization of membrane distillation membranes prepared by phase inversion, Desalination 100 (1995) 139-148.
[9] A. Bottino, G. Capannelli, O. Monticelli, P. Piaggio, Poly(vinylidene fluoride) with improved functionalization for membrane production, J. Membr. Sci. 166 (2000) 23-29.
[10] P. Martins, A.C. Lopes, S. Lanceros-Mendez, Electroactive phases of poly(vinylidene

fluoride): determination, processing and applications, Prog. Polym. Sci. 39 (2014) 683-706.
[11] F. Liu, M.-m. Tao, L.-x. Xue, PVDF membranes with inter-connected pores prepared via a Nat-ips process, Desalination 298 (2012) 99-105.
[12] M. Gu, J. Zhang, X. Wang, H. Tao, L. Ge, Formation of poly(vinylidene fluoride) (PVDF) membranes via thermally induced phase separation, Desalination 192 (2006) 160-167.
[13] X. Li, X. Lu, Morphology of polyvinylidene fluoride and its blend in thermally induced phase separation process, J. Appl. Polym. Sci. 101 (2006) 2944-2952.
[14] R. Magalhães, N. Durães, M. Silva, J. Silva, V. Sencadas, G. Botelho, J.L. Gómez Ribelles, S. Lanceros-Méndez, The role of solvent evaporation in the microstructure of electroactive β-poly(vinylidene fluoride) membranes obtained by isothermal crystallization, Soft Mater. 9 (2010) 1-14.
[15] M.L. Yeow, Y.T. Liu, K. Li, Morphological study of poly(vinylidene fluoride) asymmetric membranes: effects of the solvent, additive, and dope temperature, J. Appl. Polym. Sci. 92 (2004) 1782-1789.
[16] C. Ribeiro, V. Sencadas, J.L.G. Ribelles, S. Lanceros-Méndez, Influence of processing conditions on polymorphism and nanofiber morphology of electroactive poly(vinylidene fluoride) electrospun membranes, Soft Mater. 8 (2010) 274-287.
[17] M.G. Buonomenna, P. Macchi, M. Davoli, E. Drioli, Poly(vinylidene fluoride) membranes by phase inversion: the role the casting and coagulation conditions play in their morphology, crystalline structure and properties, Eur. Polym. J. 43 (2007) 1557-1572.
[18] X. Wang, L. Zhang, D. Sun, Q. An, H. Chen, Formation mechanism and crystallization of poly(vinylidene fluoride) membrane via immersion precipitation method, Desalination 236 (2009) 170-178.
[19] G.T. Caneba, R. Saxena, Analysis of polymer membrane formation through spinodal decomposition. Part 4: computer simulation of early-stage coarsening, Polym. Eng. Sci. 36 (1996) 288-297.
[20] D.B. Mosqueda-Jimenez, R.M. Narbaitz, T. Matsuura, G. Chowdhury, G. Pleizier, J.P. Santerre, Influence of processing conditions on the properties of ultrafiltration membranes, J. Membr. Sci. 231 (2004) 209-224.
[21] L.-P. Cheng, Effect of temperature on the formation of microporous PVDF membranes by precipitation from 1-octanol/DMF/PVDF and water/DMF/PVDF systems, Macromolecules 32 (1999) 6668-6674.
[22] T.-H. Young, J.-H. Huang, W.-Y. Chuang, Effect of evaporation temperature on the formation of particulate membranes from crystalline polymers by dry-cast process, Eur. Polym. J. 38 (2002) 63-72.
[23] M. Zhang, A.-Q. Zhang, B.-K. Zhu, C.-H. Du, Y.-Y. Xu, Polymorphism in porous poly(vinylidene fluoride) membranes formed via immersion precipitation process, J. Membr. Sci. 319 (2008) 169-175.
[24] P. Altevogt, O.A. Evers, J.G.E.M. Fraaije, N.M. Maurits, B.A.C. van Vlimmeren, The MesoDyn project: software for mesoscale chemical engineering, J. Mol. Struct. THEOCHEM 463 (1999) 139-143.
[25] S.C. Glotzer, W. Paul, Molecular and mesoscale simulation methods for polymer materials, Annu. Rev. Mater. Res. 32 (2002) 401-436.
[26] A. California, V.F. Cardoso, C.M. Costa, V. Sencadas, G. Botelho, J.L. Gómez-Ribelles, S. Lanceros-Mendez, Tailoring porous structure of ferroelectric poly(vinylidene fluo-ride-trifluoroethylene) by controlling solvent/polymer ratio and solvent evaporation rate, Eur. Polym. J. 47 (2011) 2442-2450.
[27] R.G. Petschek, H. Metiu, A computer simulation of the time-dependent

GinzburgLandau model for spinodal decomposition, J. Chem. Phys. 79 (1983) 3443-3456.
[28] D.-J. Lin, C.-L. Chang, F.-M. Huang, L.-P. Cheng, Effect of salt additive on the formation of microporous poly(vinylidene fluoride) membranes by phase inversion from $LiClO_4$ /water/DMF/PVDF system, Polymer 44 (2003) 413-422.
[29] A.C. Lopes, C.M. Costa, C.J. Tavares, I.C. Neves, S. Lanceros-Mendez, Nucleation of the electroactive γ phase and enhancement of the optical transparency in low filler content poly(vinylidene)/clay nanocomposites, J. Phys. Chem. C 115 (2011) 18076-18082.
[30] R. Gregorio, E.M. Ueno, Effect of crystalline phase, orientation and temperature on the dielectric properties of poly (vinylidene fluoride) (PVDF), J. Mater. Sci. 34 (1999) 4489-4500.
[31] A. Salimi, A.A. Yousefi, Analysis method: FTIR studies of β-phase crystal formation in stretched PVDF films, Polym. Test. 22 (2003) 699-704.
[32] S. Lanceros-Méndez, J.F. Mano, A.M. Costa, V.H. Schmidt, FTIR and DSC studies of mechanically deformed β-PVDF films, J. Macromol. Sci. B 40 (2001) 517-527.
[33] D.C. Bassett, Developments in Crystalline Polymers, Applied Science Publishers, 1982.
[34] D.L. Chinaglia, R. Gregorio, J.C. Stefanello, R.A. Pisani Altafim, W. Wirges, F. Wang, R. Gerhard, Influence of the solvent evaporation rate on the crystalline phases of solution-cast poly(vinylidene fluoride) films, J. Appl. Polym. Sci. 116 (2010) 785-791.
[35] J.R. Gregorio, M. Cestari, Effect of crystallization temperature on the crystalline phase content and morphology of poly(vinylidene fluoride), J. Polym. Sci. B Polym. Phys. 32 (1994) 859-870.
[36] J.W.M. Prest, D.J. Luca, The morphology and thermal response of high-temperaturecrystallized poly(vinylidene fluoride), J. Appl. Phys. 46 (1975) 4136-4143.
[37] C. Marega, A. Marigo, Influence of annealing and chain defects on the melting behaviour of poly(vinylidene fluoride), Eur. Polym. J. 39 (2003) 1713-1720.
[38] L. Yan, Y.S. Li, C.B. Xiang, S. Xianda, Effect of nano-sized Al_2O_3-particle addition on PVDF ultrafiltration membrane performance, J. Membr. Sci. 276 (2006) 162-167.
[39] I.M. Ward, J. Sweeney, An Introduction to the Mechanical Properties of Solid Polymers, Wiley, 2005.
[40] C.M. Costa, V. Sencadas, I. Pelicano, F. Martins, J.G. Rocha, S. Lanceros-Mendez, Microscopic origin of the high-strain mechanical response of poled and non-poled poly(vinylidene fluoride) in the β-phase, J. Non-Cryst. Solids 354 (2008) 3871-3876.
[41] J.S. Higgins, J.E.G. Lipson, R.P. White, A simple approach to polymer mixture miscibility, Philos. Trans. R. Soc. A Math. Phys. Eng. Sci. 368 (2010) 1009-1025.
[42] S. Enders, B.A. Wolf, Polymer Thermodynamics: Liquid Polymer-Containing Mixtures, Springer, 2011.
[43] M. Rubinstein, R.H. Colby, Polymer Physics, Oxford University Press, USA, 2003.
[44] L.M. Robeson, Polymer Blends: A Comprehensive Review, Hanser, 2007.
[45] J.E. Mark, Polymer Data Handbook, Oxford University Press, USA, 2009.
[46] P.K. Chan, A.D. Rey, A numerical method for the nonlinear Cahn-Hilliard equation with nonperiodic boundary conditions, Comput. Mater. Sci. 3 (1995) 377-392.